High Cycle Fatigue Life Assessment of Notched Components with Induced Compressive Residual Stress

Xuran Xiao[a*], Volodymyr Okorokov[b], Donald Mackenzie[a]

[a]Department of Mechanical & Aerospace Engineering, University of Strathclyde, Glasgow, UK

[b]Weir Minerals Netherlands, Venlo, NL

*Corresponding author, E-mail address: *xuran.xiao.2017@uni.strath.ac.uk*

Abstract

A method for predicting the high cycle fatigue life of cyclically loaded components with induced residual stress based on standard *S*-*N* curve data, a fracture mechanics crack growth model, and Finite Element Analysis using the ANSYS SMART crack growth modelling tool is proposed. The method is appropriate to high cycle fatigue analysis of components in which the working stress cycle is linear elastic and the conditions required by LEFM and the SMART FEA method are satisfied. The total fatigue life of the component is calculated as the sum of the crack initiation life and crack propagation life. Crack initiation life is evaluated for an assumed initiation crack length by reference to an *S*-N_i curve relating stress amplitude to number of cycles to crack initiation, generated from standard *S*-*N* data and application of SMART FEA to determine the crack growth component of total test specimen life. Crack propagation life is evaluated by superposition of the individual applied load and residual stress fields, where variation in stress intensity factor with increasing crack length is obtained in the form of polynomial equations. Numerical and experimental investigation of double-notch 316L stainless steel tensile specimens show that the proposed method gives an improved estimate of fatigue life when compared to standard stress-life fatigue assessment for specimens both with and without induced compressive residual stress.

Keywords:

Crack initiation, Crack propagation, Residual stress, Fatigue life prediction

This is a peer-reviewed, accepted manuscript of the following paper: MacKenzie, D., Xiao, X., & Okorokov, V. (2023). High cycle fatigue life assessment of notched components with induced compressive residual stress. International Journal of Pressure Vessels and Piping, 206, Article 105069. https://doi.org/10.1016/j.ijpvp.2023.105069

1 Introduction

Autofrettage is a pre-stressing technique used to enhance the fatigue life of pressurised components under repeated or cyclic loading, such as pressure vessels, high pressure pump bodies, diesel engine common rail injectors and gun barrels [1]. Fatigue failure of these components usually occurs by crack initiation and growth at local stress raising features, referred to as notches, on the pressurised surface of the component. In the autofrettage process, compressive residual stress is induced at these locations prior to service through controlled over-pressurisation of the component. This causes limited plastic deformation in high stress regions, which prevents full elastic recovery on unloading, resulting in a self-equilibrating residual stress system in the component with local compressive stress in the notch regions. When the component is subsequently subjected to varying operating pressure in service, the compressive residual stress has the effect of reducing the mean stress at the notch and increasing the fatigue life of the component.

High cycle fatigue failure of engineering components is commonly assessed using the stress-life method, based on linear elastic calculation of a nominal stress S at the point of investigation and fatigue data in the form of *S*-*N* curves (stress vs number of cycles to failure) for smooth, notch-free specimens [2]. This approach becomes more complicated when notches and residual stress are present in the component. Notches are known to reduce fatigue life, but stress life assessment based on the maximum elastically calculated stress at the notch can be over-conservative, particularly for sharp notches. This notch effect is attributed to the local stress gradient at the notch. This effect can be accounted for in stress-life calculations by defining the nominal stress with reference to a finite volume of material in the notch region, through methods such as Neuber's method [3], Peterson's method [4], and the theory of critical distance (TCD) [5, 6].

For arbitrary constant R, mean stress correction approaches such as Goodman, Gerber and Soderberg mean stress correction can be applied to calculate a nominal stress ($R = -1$) to predict the fatigue life from *S*-*N* curves [7]. In the TDC, the nominal stress is based on a material characteristic length, defined in terms of the plain specimen fatigue limit and the threshold value of stress intensity factor range, both of which are dependent on the ratio of maximum to minimum stress, R, over the applied load cycle. In the TDC, R is assumed to be constant over the characteristic length. However, when a component has been subject to autofrettage prior to operation, the compressive residual stress changes the stress gradient at

the notch. Consequently R varies over the characteristic length and the TCD approach is not directly applicable [8].

A similar problem arises in fracture mechanics assessment of fatigue life. Linear Elastic Fracture Mechanics, LEFM, provides an alternative to the stress life method for calculating fatigue life. In a basic LEFM procedure, the fatigue process can be considered in two stages, crack initiation and crack propagation. The total fatigue life N_t is the sum of the crack initiation life N_i and the fatigue crack growth life N_g:

$$N_t = N_i + N_g \tag{1}$$

Crack initiation is associated with nucleation and propagation of Microstructurally Short Cracks, MSC, and Physically Short Cracks, PSC. The basic LEFM approach does not model crack initiation life, for which more advanced approaches are required [9, 10]. However, crack growth life N_g can be determined analytically from a crack growth model such as the Paris Law [11]:

$$\frac{da}{dN} = C(\Delta K)^m \tag{2}$$

where, a is crack length, N is number of cycles, ΔK is the stress intensity factor range and C and m are material parameters.

Crack propagation can also be modelled numerically in a Finite Element environment, using methods such as Cohesive Zone Modeling (CZM) [12], Extended Finite Element Method (XFEM) [13, 14], and ANSYS Separating Morphing and Adaptive Remeshing Technology (SMART) [15-17]. These analytical and numerical approaches are straightforward when the stress ratio R is constant but more problematic when R varies with crack length, as is the case when compressive residual stress is present. For example, to calculate the crack growth life using the SMART crack growth method, the total crack propagation is divided into several substeps and the crack growth life of each substep is calculated by the Paris law. However, due to the residual stress distribution the value of R in each substep is different, and the values of the Paris law parameters C and m are dependent on R. Therefore, the completed crack growth life cannot be determined by a single value of R, and most current studies applying SMART crack growth method do not consider the presence of residual stress [15-17].

Several models have been proposed in the literature for crack growth in the presence of induced residual stress. These mainly focus on determining the stress intensity factor for the residual

stress field, K_{rs} which may be calculated by a weight function approach, proposed by Buechner [18] as:

$$K_{rs} = \int_{x=0}^{x=a} \sigma_{rs} m(x,a) dx \tag{3}$$

where, a is crack length, σ_{rs} is residual stress and $m(x,a)$ is the weight function. The basis of the weight function method is to calculate the stress intensity factors from the stress distribution around the crack, rather than from the remote loading. Weight functions for edge cracks can be obtained from constant and linear crack face pressure fields [19] and have been obtained for different combinations of cracks and structures [20]. However, the weight function method may be difficult to apply to complex 3D structures such as pressure vessel, pumps or valves [21].

This paper proposes a methodology for high cycle fatigue life analysis of notched components with compressive residual stress based on smooth fatigue specimen *S-N* data, an assumed crack initiation length based on material grain size, a fracture mechanics crack growth model, and Finite Element Analysis using the ANSYS SMART crack growth modelling tool. The proposed method is applied in an investigation of the fatigue life of preloaded double-notch test specimens of AISI 316L austenitic stainless steel. The specimen design is such that compressive residual stress can be induced in the notch region through controlled axial overload prior to fatigue testing [8], resulting a local compressive stress distribution similar in form to that commonly found at stress raisers in pressure-components after autofrettage.

2 Methodology

The fatigue crack model used in the present study combines a stress life method for crack initiation life based on an assumed initial crack length and a LEFM model for crack propagation in the presence of compressive residual stress. The residual stress is determined by elastic-plastic finite element analysis and exported to the LEFM model, such that the stress intensity factor of residual stress can be determined by superposition.

2.1 Crack Initiation

Crack initiation life can be a significantly part of the total fatigue life, especially for high cycle fatigue [22]. Application of advanced fracture mechanics models for crack initiation is not always practical for analysis of complex engineering components. An alternative approach is to adopt a stress life approach in which the end of initiation is defined as the development of a specific MSC length, and N_i as the number of cycles required for the crack to initiate and grow

to this length. This approach requires fatigue test data in the form of S-N_i curves for a specific initiation length, rather than complete fracture of the specimen [23]. However, in practice, it is difficult to measure the number of cycles required to reach a specific crack length directly (typically requiring scanning electron microscopy, etc.), and most *S-N* curves are based on complete fracture of the specimen.

Investigations of microstructurally small crack growth [24-26] show that in the initiation stage several fatigue cracks originate from persistent slip bands and then stretch across one grain. Most cracks stop at the grain boundary, as the crack can only extend further when adjacent grains have similar orientation. This observation provides a basis for estimating the initial fatigue crack length, in that it must span at least two grains of material. 316L stainless steel, which is widely used in the production of pressure vessels, pumps and valves [27, 28], is used in this study as a reference material to investigate the validity of the proposed method of fatigue life assessment. In an investigation of micro-cracks in 316L stainless steel, Obrtlik et al. [24] defined a crack transition length a_t, which divided the fracture into a crack generation region and a crack propagation region. Crack generation was limited by reaching a_t, which can be assumed to be the length two average grains. The average grain length in their investigation was $100\mu m$. The assumed initial crack length for 316L is therefore $200\mu m$. For other materials, the assumed initial crack length will be dependent on the grain size of the specific material and must be defined on a material-by-material basis.

2.2 Calculating the S-N_i Curve

In the proposed method, the crack initiation life is determined by a stress life method based on a derived stress vs number of cycles to crack initiation, S-N_i, curve for smooth fatigue specimens. A conventional *S-N* curve defines the total number of cycles to specimen failure, encapsulating the crack initiation life and crack propagation life. Here, the crack initiation life is determined by calculating the crack propagation life for an assumed initial crack length and subtracting this from the total fatigue life.

Considering AISI 316L stainless steel, the average size of two grains is selected as the crack initiation length based on experimental observations from [26], as discussed in section 2.1. The assumed initial crack length of $200\mu m$ broadly agrees with the TCD methodology [6], where cracks are assumed to emanate from a length equal to two material characteristic lengths ($224\mu m$ for AISI 316L).

Huang et al. [29] performed fatigue tests for 316L with load ratio $R = 0.2$ for a plain cylindrical tensile test specimen following ASTM E466 [30], presenting the results as a maximum stress (S_{max})-total fatigue life (N_t) curve. Here, a corresponding S-N_i curve corresponding to a 200μm crack initiation length is derived from this data by calculating the crack growth life using the ANSYS SMART tool.

ANSYS SMART is an Unstructured Mesh Method in which initial cracks can be defined at any location in a component. This has been used in several recent investigations of fatigue failure [15-17]. Here, a SMART crack growth finite element model of the test specimen of Huang et al. was created in ANSYS Workbench. In a conventional 2D crack finite element model, the crack is meshed radially due to the singularity around the crack-front [31]. In a SMART crack model, the entire structure is meshed with 3D SOLID187 10 node tetrahedral structural solid elements, with mesh refinement at the crack front. Following a convergence study, an initial mesh of 20,991 elements (33,283 nodes) graduated towards the central region of the specimen as shown in Figure 1, was selected. During crack propagation, the SMART tool can automatically re-mesh the crack-front region.

The material properties were Young's modulus E=200GPa, Poisson's ratio $\nu = 0.3$ and Paris Law constants $C = 5.61\text{x}10^{-9}\ \frac{\text{mm / cycle}}{(MPa\sqrt{\text{m}})^m}$ and $m = 3.25$ [32]. The model was fully fixed at one end, and a uniformly distributed axial cyclic force of 70MPa applied at the free end.

An initial semi-elliptical crack of length 200μm was located in the central section of the model. From previous investigations of the shape of surface cracks in round bars under constant axial loading [33, 34], the crack minor to major axis aspect ratio was defined as 0.6.

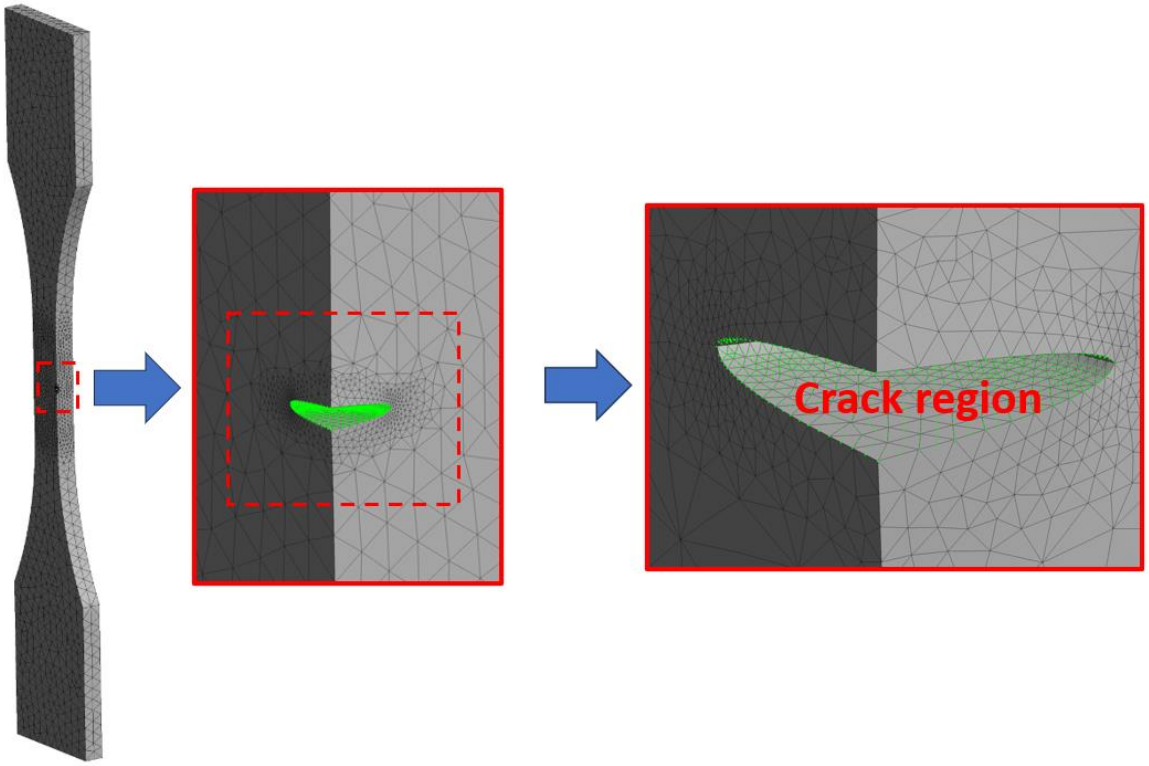

Figure 1. Finite element model of cracked smooth specimen, showing the overall finite element mesh and zoomed view of the crack region.

The SMART facility was used to calculate the number of cycles to failure N_g during crack growth for a given axial stress cycle $\Delta\sigma_n$. The corresponding crack initiation life was then calculated from the S_{max}-N_t curve of [29], such that $N_i = N_t - N_g$. The S-N_i curve can generated by repeating the SMART analysis for several different load magnitudes. Alternatively, a more computationally efficient approach can be used, in which a single SMART analysis is performed to obtain the variation of stress intensity factor range ΔK with increasing crack length a for a nominal stress range $\Delta\sigma_n$. ΔK can then be defined as a continuous function of a by fitting a polynomial equation of order n to the numerical results, such that:

$$\Delta K = f(a) = A_n a^n + A_{n-1} a^{n-1} + \cdots + A_0 a^0 \tag{4}$$

where $A_n, A_{n-1}, \ldots, A_o$ are constants. A corresponding function for configuration factor Y is thus defined as:

$$Y(a) = \frac{1}{\Delta\sigma_n \sqrt{\pi a}} f(a) \tag{5}$$

The fatigue life for any stress range $\Delta\sigma$ can then be determined analytically from the Paris law in the form:

$$\frac{da}{dN_g} = C(\Delta K_{\Delta\sigma})^m \tag{6}$$

where

$$\Delta K_{\Delta\sigma} = Y(a)\sqrt{\pi a}\,\Delta\sigma \tag{7}$$

The crack growth life N_g for stress range $\Delta\sigma$ is thus:

$$N_g = \int_{a_0}^{a_f} \frac{1}{C(K_{\Delta\sigma})^m} \tag{8}$$

where a_0 and a_f are initial crack length and final crack length respectively.

Figure 2 shows the generated stress-initiation life, *S*-N_i, curve for 316L based on 5 different load levels, along with the original total fatigue life *S*-*N* curve from [29]. This shows that the proportion of crack initiation life to total life declines with increasing maximum stress. This trend agrees with results from Santus and Taylor, who numerically calculated N_i through physically short crack propagation in several metals [22]. From this trend, $log\ (N_i)$ can be assumed to vary linearly with maximum stress in the high cycle fatigue range.

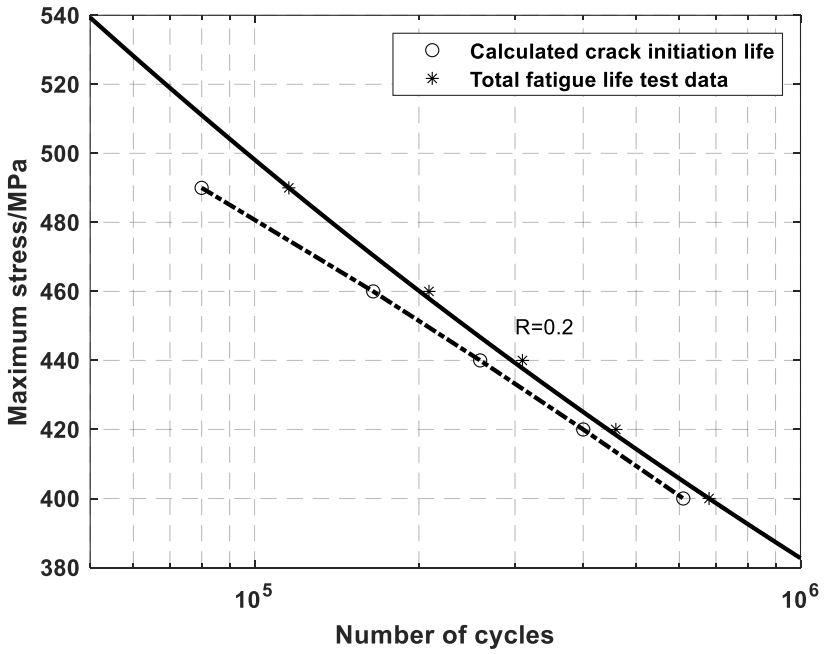

Figure 2. Total life curve (R=0.2) [29] and proposed stress-crack initiation life.

2.3 Residual Stress Effect

Two approaches have been proposed in the literature to represent the influence of K_{rs} on crack propagation: the crack closure method [35, 36] and the superposition method [37].

In the crack closure approach, Elber proposed that the closure and opening of a crack is controlled by the effective stress intensity factor range, ΔK_{eff}. The crack will not propagate unless the effective stress intensity factor is larger than the opening stress intensity factor. ΔK_{eff} can thus be treated as a function of the stress intensity factor range, ΔK, and stress intensity factor ratio R [36]. Crack-growth rates $\frac{d_a}{d_N}$ with ΔK curves for different values of R can then be replaced by a single curve by adopting an appropriate mean stress model. The relationship between $\frac{d_a}{d_N}$ and ΔK_{eff} can thus be determined in the form of the Paris law.

In the superposition method, the total stress intensity factor K_{tot} is considered as two components: the applied stress intensity factor, K_{app}, and residual stress intensity factor K_{rs}. The maximum stress intensity factor, $K_{max,tot}$, and minimum stress intensity factor $K_{min,tot}$ are thus:

$$K_{max,tot} = K_{max,app} + K_{rs} \tag{9}$$

$$K_{min,tot} = K_{min,app} + K_{rs} \tag{10}$$

The total stress intensity factor range ΔK_{tot} is therefore:

$$\Delta K_{tot} = K_{max,tot} - K_{min,tot} = K_{max,app} + K_{rs} - K_{min,app} - K_{rs}$$

which is independent of the residual stress and equal to ΔK_{app}:

$$\Delta K = K_{max,app} - K_{min,app} = \Delta K_{app} \tag{11}$$

The effective stress intensity ratio R_{eff} can then be obtained as:

$$R_{eff} = \frac{K_{min,tot}}{K_{max,tot}} = \frac{K_{min,app} + K_{rs}}{K_{max,app} + K_{rs}} \tag{12}$$

2.4 Determining K_{rs} by Superposition

The effect of induced residual stress on crack growth is determined using the superposition method. This requires evaluation of $\Delta K = \Delta K_{app}$ (11) and R_{eff} (12). As the weight function method is difficult to apply in complex 3D models, a numerical method based on the superposition method is proposed to calculate K_{rs}.

The residual stress distribution in the component under investigation is evaluated by elastic-plastic FEA for a given initial autofrettage overload. As the SMART tool is restricted to linear elastic material behaviour, it cannot be applied in a plastically deformed model. However, the effect of residual stress on crack propagation can be represented by importing the calculated residual stress distribution into a similar linear elastic model as an initial state of stress.

Two linear elastic models with identical meshes are used to determine the stress intensity factor of the residual stress K_{rs}. The first model considers the component with no autofrettage. The elastic model is subject to an applied cyclic load P_{app}, representing the operating conditions of the component. The stress intensity range calculated with increasing crack length using this model is ΔK_{app}. In the second condition, the residual stress calculated in the elastic-plastic solution is imported into the elastic model as an initial state of stress, and cyclic load P_{app} applied. The stress intensity range calculated by this model is $\Delta K_{app} + K_{rs}$. The variation of the stress intensity of the residual stress K_{rs} with crack length a is then evaluated by stress superposition, by subtracting ΔK_{app} from the second condition results.

2.5 Correlating Paris Law with K_{rs}

In the superposition approach, the crack growth rate is defined as a function of ΔK_{eqv} and R_{eff}:

$$\frac{da}{dN} = C_{R_{eff}} \left(\Delta K_{eqv}\right)^{m_{R_{eff}}} \tag{13}$$

where $C_{R_{eff}}$ and $m_{R_{eff}}$ are the Paris law parameters corresponding to stress ratio R_{eff}. The value of R_{eff} varies during crack growth, and therefore Paris law parameters for several values of R are required. The Walker equation is applied in the SMART crack growth method to corelate the Paris law with R and calculate ΔK_{eqv} from ΔK_{app}, without the crack closure effect. However, when considering the influence of the compressive residual stress, the values of R_{eff} in the compressive residual stress region are always negative, in which case the values of K_{max} better define the crack closure and opening effect, compared with ΔK based on the crack closure concept.

Kujawski [38] addressed the crack closure effect by correlating the fatigue crack growth rate with a variable stress ratio R. The driving force for crack growth may depend on the material properties, temperature, and environment. For example, in a ductile material the driving force is dominated by ΔK, but in a brittle material it is controlled by K_{max}. Kujawski proposed a new form of crack driving force, K^*, combining ΔK and K_{max}:

$$K^* = (K_{max})^{\alpha}(\Delta K^+)^{1-\alpha} \tag{14}$$

where α is a correlation parameter, $\Delta K^+ = \Delta K$ when R$\geq$ 0 and $\Delta K^+ = K_{max}$ when R$<$ 0.

On this basis, the stress intensity factor range ΔK in the Paris equation is replaced by K^*, and the effect of R is incorporated by:

$$\Delta K = K^*(1-R)^{\alpha} \qquad \text{For } R > 0 \tag{15}$$

$$\Delta K = K^*(1-R) \qquad \text{For } R < 0 \tag{16}$$

The Paris law is thus correlated as:

$$\frac{da}{dN} = C_{R=0}[\frac{\Delta K}{(1-R)^{\alpha}}]^{m_{R=0}} \qquad \text{For } R > 0 \tag{17}$$

$$\frac{da}{dN} = C_{R=0}[\frac{\Delta K}{(1-R)}]^{m_{R=0}} \qquad \text{For } R < 0 \tag{18}$$

Kujawski's equations include the crack closure effect. Based on Kujawski's approach, two extended equations are proposed to calculate the crack growth life, combining the values of K_{app} and K_{rs} and considering the intervals with different values of R. The crack growth rate in the presence of induced residual stress is obtained by substituting ΔK_{app} from (11) and R_{eff} from (12) into (17) and (18). The number of cycles to grow a crack from initial length a_0 to final length a_f is thus:

$$\mathrm{N} = \int_{a_0}^{a_f} \frac{1}{C\left(\frac{\Delta K}{(1-R)^{\alpha}}\right)^{m}} = \int_{a_0}^{a_f} \frac{1}{C\left(\frac{K_{app}}{\left(1-\frac{K_{rs}}{K_{app}+K_{rs}}\right)^{\alpha}}\right)^{m}} \qquad \text{For } R > 0 \tag{19}$$

$$N = \int_{a_0}^{a_f} \frac{1}{C(\frac{\Delta K}{(1-R)})^{m}} = \int_{a_0}^{a_f} \frac{1}{C(\frac{K_{app}}{\left(1-\frac{K_{rs}}{K_{app}+K_{rs}}\right)})^{m}} \qquad \text{For } R < 0 \tag{20}$$

In the proposed method, these equations are limited to high cycle fatigue analysis, in which the stress cycle under external loading is linear elastic and the applied stress intensity factor K_{app} is determined by LEFM.

3 Implementation

The proposed procedure for calculating the fatigue life in a notched component with an induced residual stress system defined in Section 2 is shown schematically Figure 3.

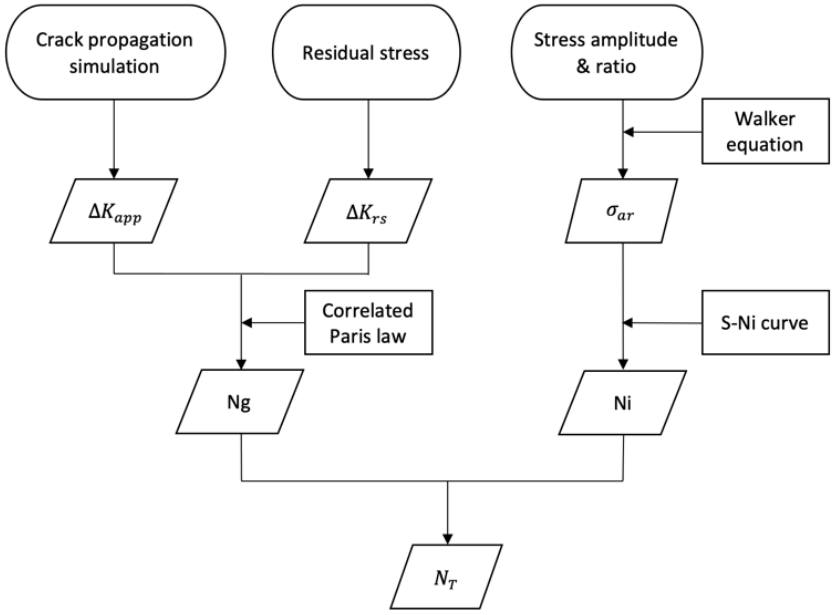

Figure 3. Flow chart for calculating total fatigue life of a component with residual stress.

Crack propagation in notched elastic components with no residual stress can be calculated directly by FEA SMART analysis, in the same way as the plain fatigue specimen in Section 2.2. When more than one load level is considered, separate SMART analyses can be performed for each load level considered. Alternatively, a polynomial representation of the stress intensity range (4) can be determined from a single SMART analysis and a continuous function for configuration factor (5) obtained. This can then be substituted into the Paris law (19) and (20) and integrated for each individual stress range considered. The latter approach requires less FEA computing resource and is used here to determine the fatigue life in regions of compressive residual stress.

3.1 Notched Specimen and Material

The fatigue life prediction method was applied to a double-notch square section tensile test specimens, shown in Figure 4. The double-notch specimen is more representative of the 3D stress distribution in pressure components with local stress raisers, such as pressure vessels, pumps bodies and valve housings, than a single notch specimen. It can also be designed to include a larger stress concentration factor, leading to higher residual stress when experimentally investigating the influence of residual stress on fatigue life.

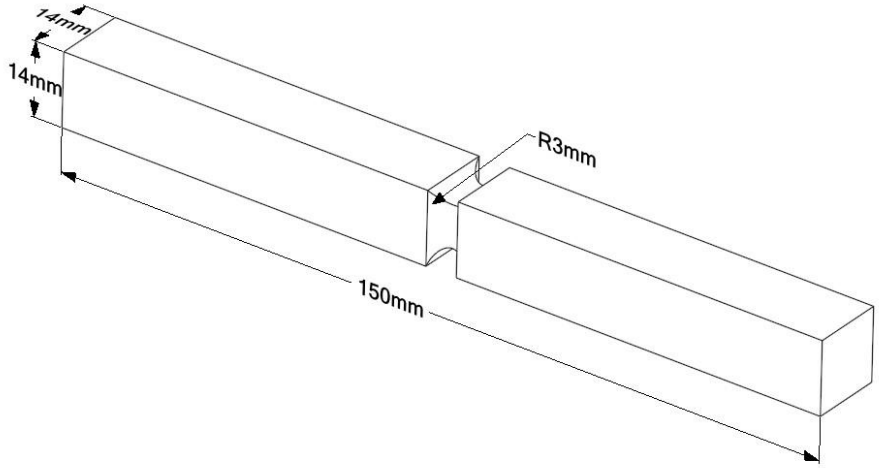

Figure 4. Double-notch fatigue test specimen.

3.2 Monotonic Material Properties

A monotonic stress-strain curve for the 316L material was obtained by tensile test. Following ASTM E8 [39], the tensile test specimen was designed as shown in Figure 5. Two monotonic stress-strain curves were obtained, as shown in Figure 6.

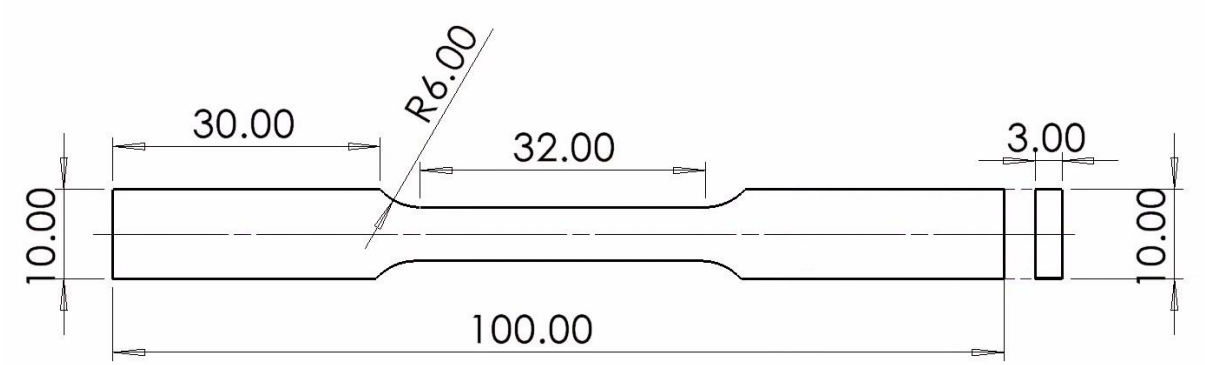

Figure 5. Tensile test specimen geometry [mm].

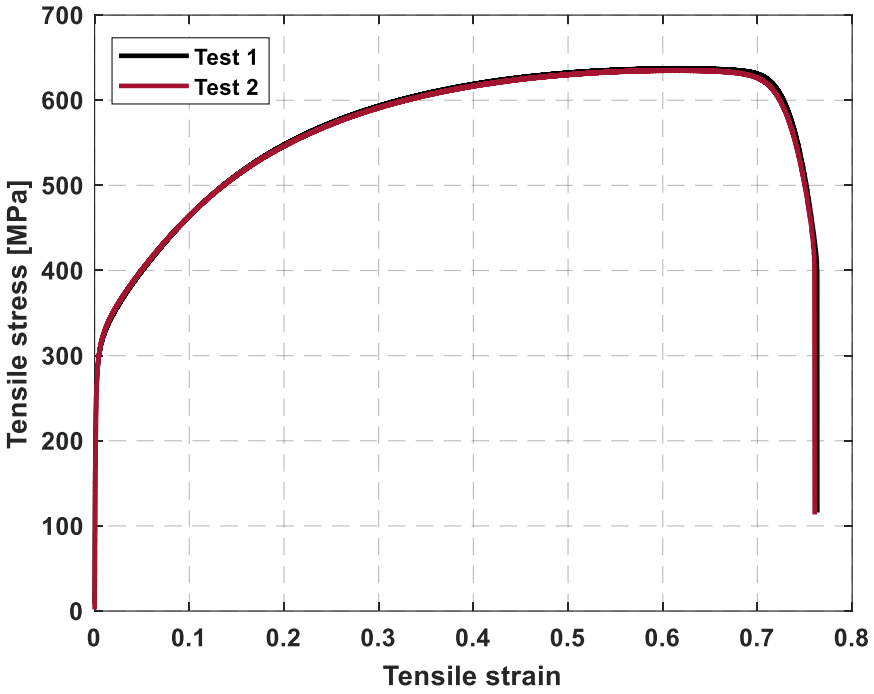

Figure 6. Monotonic stress-strain curves for two 316L specimens.

Figure 6 shows the 316L stainless steel exhibits continuous yielding. As such, there is no distinct yield point and yield stress is usually defined with reference to a specific plastic strain offset, such as the 0.2% proof stress used in general engineering. The 0.2% offset definition is not suitable for a detailed elastic-plastic analysis as presented here [40]. Alternative definitions of the offset strain [41-43] have been reviewed by Abdel-Karim, ranging from 0.01% to 0.1% [44]. In the present study, 0.01% offset strain was selected, giving a yield stress of 225MPa. Young's Modulus was obtained as 200GPa.

3.3 Cyclic Material Properties

To calculate the crack initiation life in the presence of compressive residual stress, the cyclic stress-strain curve for the material is required for use in FEA. When a ductile material is subject to cyclic loading beyond its elastic limit, its plastic flow characteristics may change due to repeated plastic deformation. The ability of the material to resist deformation may increase or decrease, known as cyclic hardening and cyclic softening respectively. In multiaxial stress, the elastic-plastic response may be represented by several plasticity models. In isotropic hardening, the yield surface remains the same shape, but expands with increasing stress. However, when a material exhibits the Bauschinger effect, the yield surface does not remain the same shape and the isotropic hardening model does not capture the cyclic response. In the linear kinematic hardening plasticity model of Prager, the yield surface maintains its size and translates in stress

space [45], giving a basic representation of the Bauschinger effect. The more advanced nonlinear kinematic hardening model of Armstrong and Frederick better captures the complete response by adding a term to model the stability of cyclic hardening behavior [46].

Chaboche [47] proposed a kinematic hardening model based on the Armstrong and Frederick model to describe the cyclic stress-strain curve:

$$\sigma_a = \sigma_Y + \sum_{i=1}^{M} \frac{C_i}{\gamma_i} \tanh\left(\gamma_i \varepsilon_{ap}\right) \tag{21}$$

where, σ_a is stress amplitude and ε_{ap} is plastic strain amplitude in the hysteresis loop and C and γ are material constants: the initial hardening modulus and the rate of reduction of the hardening modulus respectively. Here, the Chaboche model parameters are determined from data from stable cyclic stress-strain tests of Dutta et al [48]. The four data points used to fit the model are shown in Figure 7, along with the monotonic stress-strain curve from the present investigation (Figure 6). Comparison of the monotonic and cyclic stress-strain data illustrates the cyclic hardening behaviour of 316L stainless steel [49].

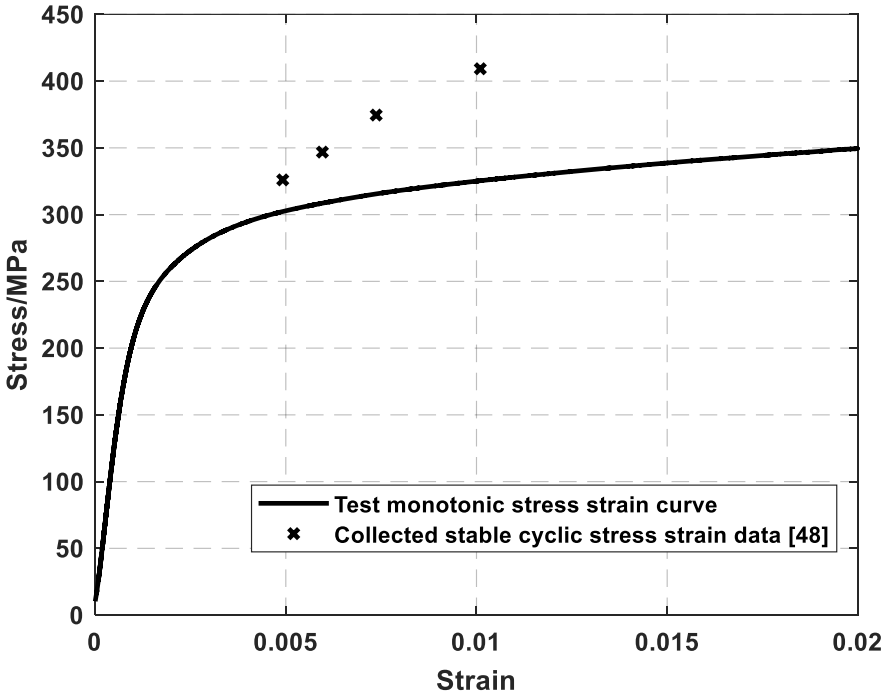

Figure 7. 316L monotonic stress-strain curve and cyclic stress-strain data from [48], showing material cyclic hardening.

4 Notched Specimen without Residual Stress

The double-notch specimen was modelled in ANSYS Workbench using the SMART crack growth tool, using SOLID 187 10 node tetrahedral structural solid elements with the mesh refined towards the crack front. An initial semi-elliptical crack with an aspect ratio of 0.6 located at the intersecting notch root of the model was considered, as shown in Figure 8. A coordinate system defined at the crack has X in the direction of the crack path and Y perpendicular to the crack surface.

Preliminary finite element investigations showed a lengthwise quarter-symmetry model of the specimen gave similar results to a full model with the same mesh density for the crack growth range considered. A quarter model was therefore used in the analysis to reduce computing requirements.

The material properties were as given in Section 2.2 for the smooth fatigue specimen model. The quarter-model was fully fixed at one end and symmetry boundary conditions applied on the planes of symmetry. Cyclic axial force varying between zero to a maximum value was applied to the free end of the model. Analysis was performed for three maximum force values, corresponding to 8kN, 8.5kN and 9kN on a full test specimen.

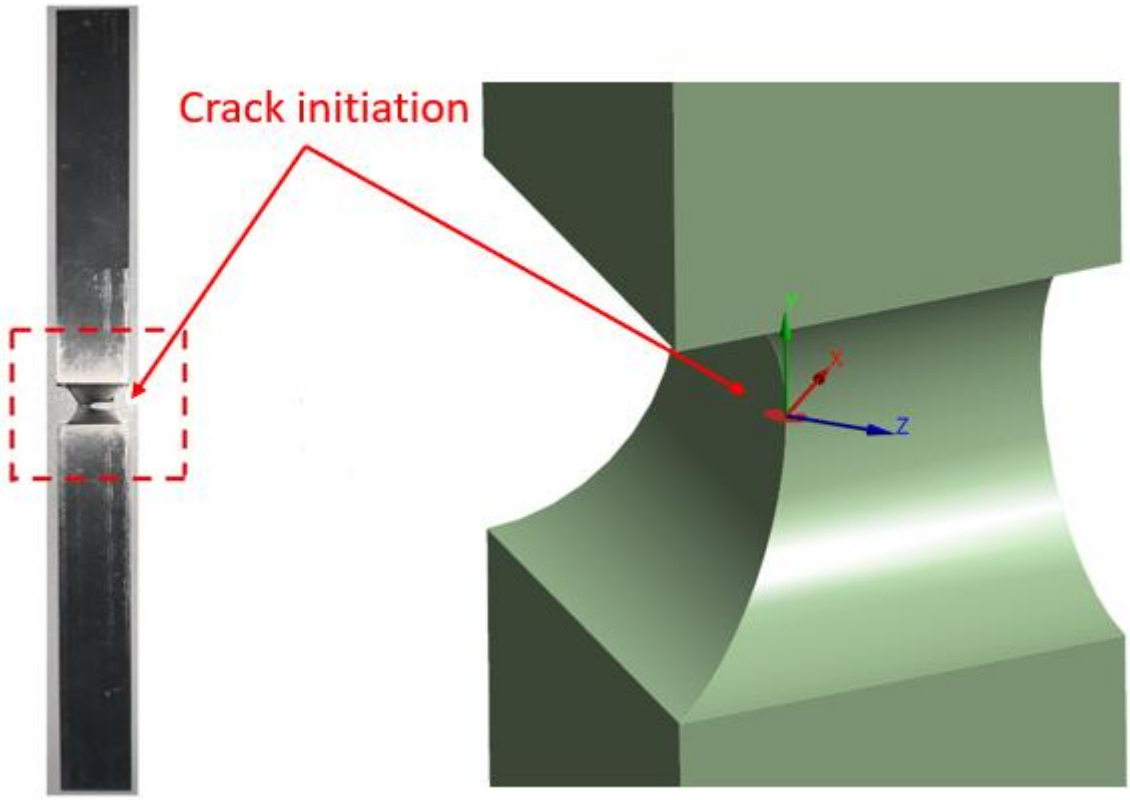

Figure 8. Failed test specimen and quarter symmetry model showing the location of crack initiation.

A convergence study was performed by investigating the effect of mesh density on the calculated configuration factor Y, (5). Results of Y distribution for two mesh density are shown in Figure 9: Mesh 1 had 28525 elements (42727 nodes) and Mesh 2, shown in Figure 10, had 14532 elements (22580 nodes). Figure 9 shows that the values of Y calculated for a range of relative crack depths are similar for both meshes. Mesh 2 was therefore selected for analysis to minimise computing requirements.

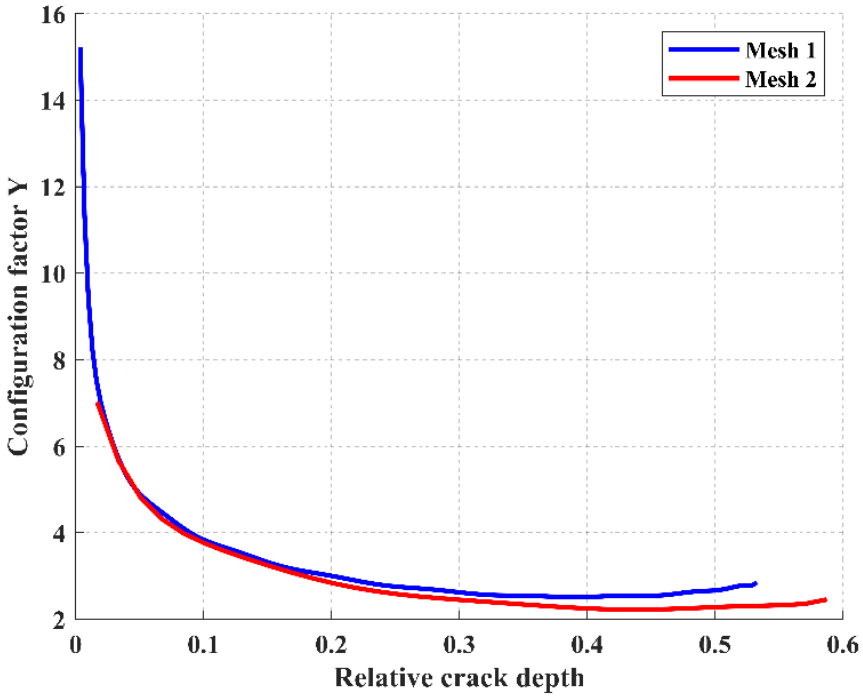

Figure 9. Configuration factor Y for a crack in the double-notch specimen for two different mesh densities.

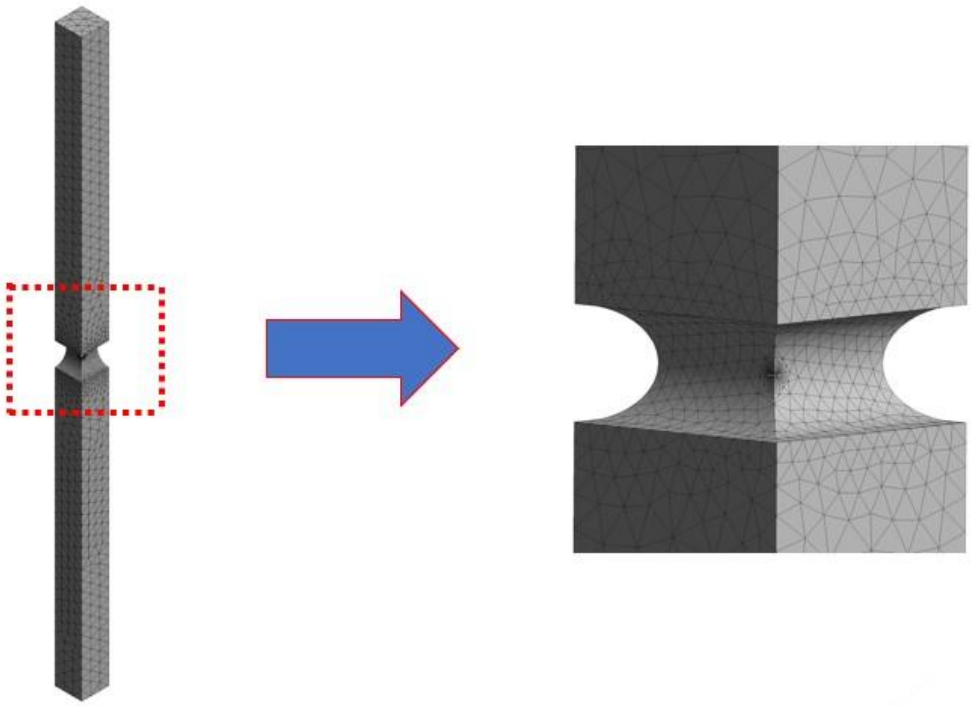

Figure 10. Finite element mesh used in analysis (Mesh 2).

Figure 9 shows that in the notched specimen Y decreases with increasing crack size, possibly due to the stress gradient, and then has a slight increase at the end. As the stress decreases with distance from the notch root, the nominal stress $\Delta\sigma_n$ in (5) varies with crack propagation and must be updated. The trend of Y in Figure 9 is similar to that of Schijve [50], who determined the stress intensity factor of cracks at notches by considering the influence of stress concentration factor.

The numerical results for ΔK_{app} obtained for the three applied loads are shown in Figure 11. As the values of ΔK_{app} are thus determined, the crack growth life without the residual stress can be calculated from the Paris law in (8).

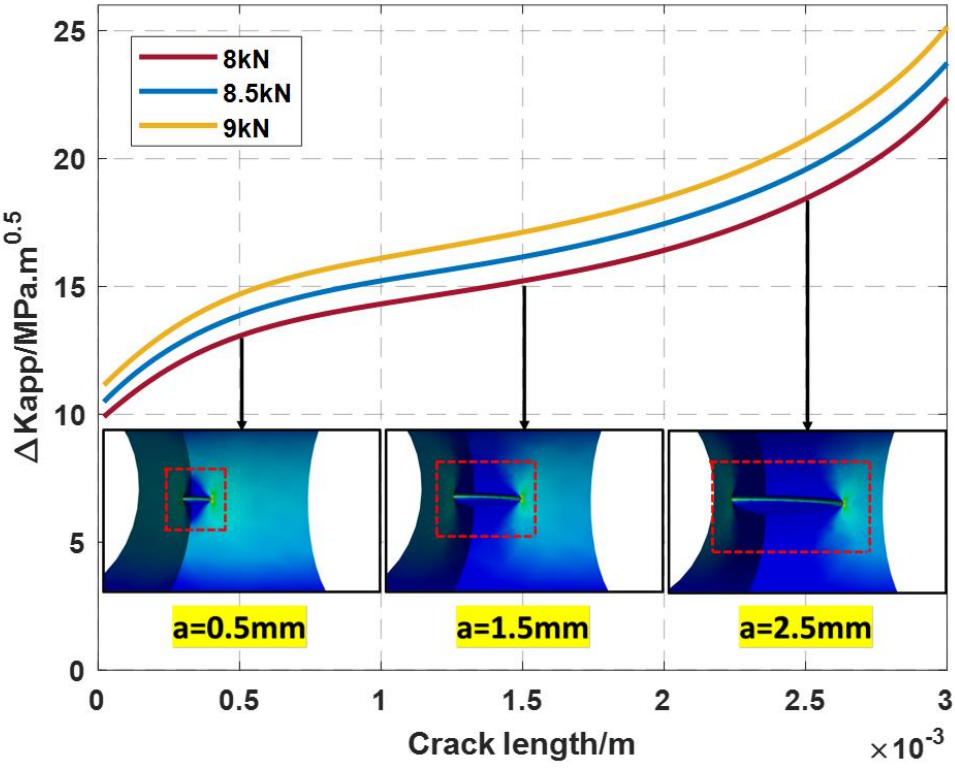

Figure 11. Variation in of stress intensity factor range ΔK_{app} with increasing crack length.

5 Notched Specimen with Residual Stress

Residual stress can be induced in double-notch specimens by tensile preloading prior to fatigue testing, causing local plastic deformation at the notch root on loading and inducing compressive residual stress on unloading.

5.1 Residual Stress Calculation

The notch root residual stress was calculated by elastic-plastic Finite Element Analysis in ANSYS workbench. A quarter-symmetry finite element model was used, with a mesh similar to the crack growth model of Section 4 prior to insertion of the SMART crack. A multilinear kinematic hardening plasticity material model based on the monotonic stress-strain curve of Figure 6 was used. The finite element model was fully fixed at one end and symmetry boundary conditions applied on the planes of symmetry. The preload was simulated by applying a uniformly distributed axial tensile force equivalent to 21kN on a full specimen to the free end of the specimen, then reducing the force to zero.

When the axial force was applied, plastic deformation occurred locally at the notch root. When the force was then reduced to zero, a compressive residual stress system was established at the notch root due to elastic recovery of the elastically deformed regions of the specimen. The

distribution of minimum principal residual stress in the notch region and along the predicted crack path are shown in Figure 12.

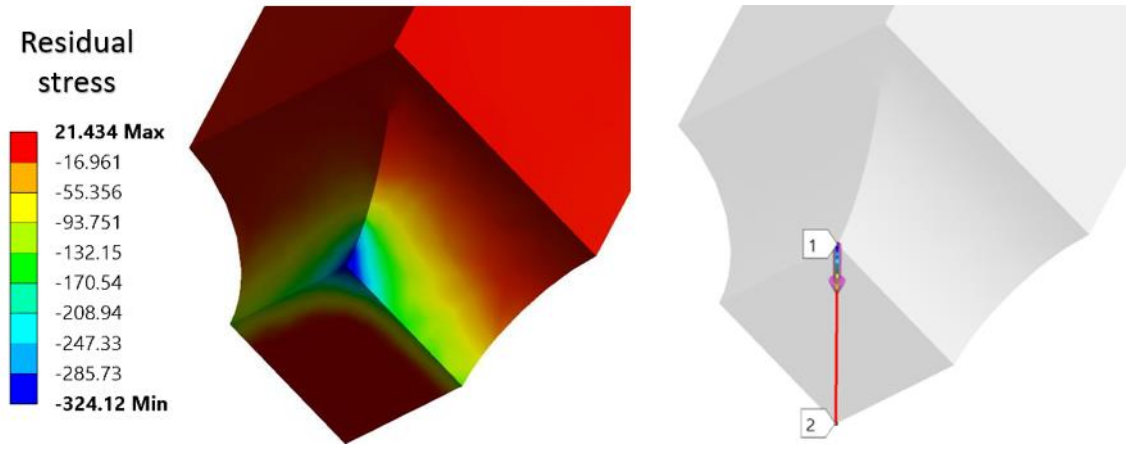

Figure 12. Minimum principal stress distribution (residual stress) at the notch root after preloading and local distribution along the crack path [MPa].

5.2 Stress Intensity Factor of Residual Stress

When the distribution of residual stress is known, K_{rs} can be calculated by treating the residual stress field as an initial condition in Finite Element Analysis. Here, a superposition method is proposed to calculate the K_{rs}, using the SMART crack growth method. First, the calculated residual stress distribution is exported from the elastic-plastic solution and imported into a similar LEFM model as an initial state of stress prior to SMART crack growth simulation. The initial crack cannot propagate with only residual stress, so crack propagation is simulated using an applied arbitrary axial load. With the arbitrary load, the value of $\Delta K_{app} + K_{rs}$ with changing crack length a is obtained and based on the superposition method, the value of K_{rs} can be determined by subtracting ΔK_{app}. The calculated variation of K_{rs} with crack length is shown in Figure 13. The values of K_{rs} can also be represented by a polynomial equation (4), and combined with the values obtained for ΔK_{app} (Figure 11) to determine the crack growth life with induced residual stress from equations (19) and (20).

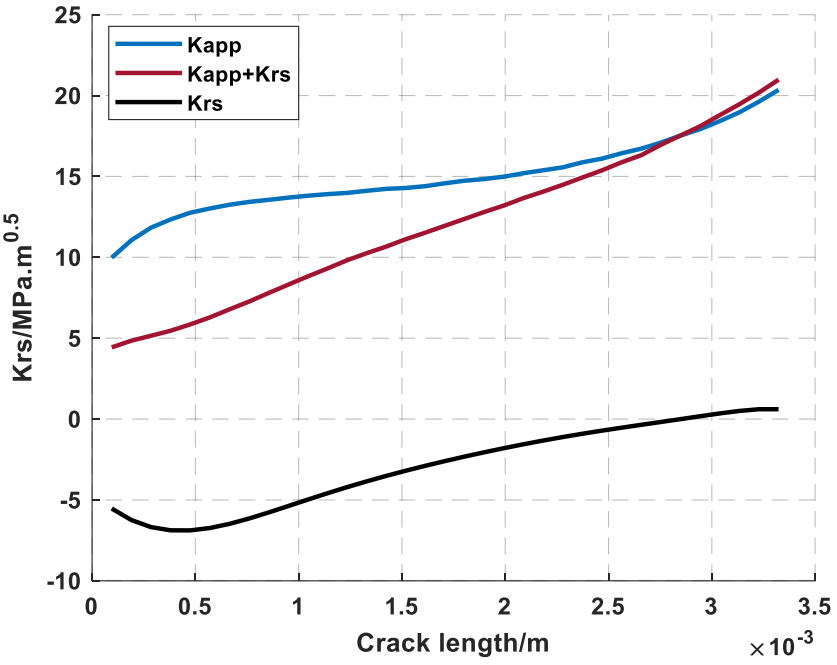

Figure 13. Stress intensity factor of residual stress against the crack length.

5.3 Crack Initiation Life Prediction

The crack initiation life is determined from the stress-crack initiation curve shown in Figure 2 by calculating the equivalent stress amplitude experienced by the specimen during cyclic loading. The equivalent stress is calculated from a FEA model similar to the preload model, but with a Chaboche kinematic hardening plasticity material with parameters $C_1 = 63400MPa$ and $\gamma_1 = 303.41$, obtained by curve-fit of the cyclic stress-strain data of Figure 7. For specimens with a preload-induced residual stress field, the residual stress distribution is exported from the original preload elastic-plastic finite element model and imported into the cyclic load model as an initial stress condition. Three different cyclic axial force amplitudes of 8kN, 8.5kN and 9kN were applied to investigate the cyclic stress behaviour for specimens.

Results for 8kN force amplitude with and without residual stress are shown in Figure 14. The maximum stress amplitude of 240.1MPa occurs at the notch root. The mean stress for the non-preloaded specimen is 74.4MPa. When the preload is included, this reduces to -0.1MPa. In the stress-life method, the decrease in mean stress leads to a lower equivalent stress amplitude, increasing the calculated fatigue life of the specimen.

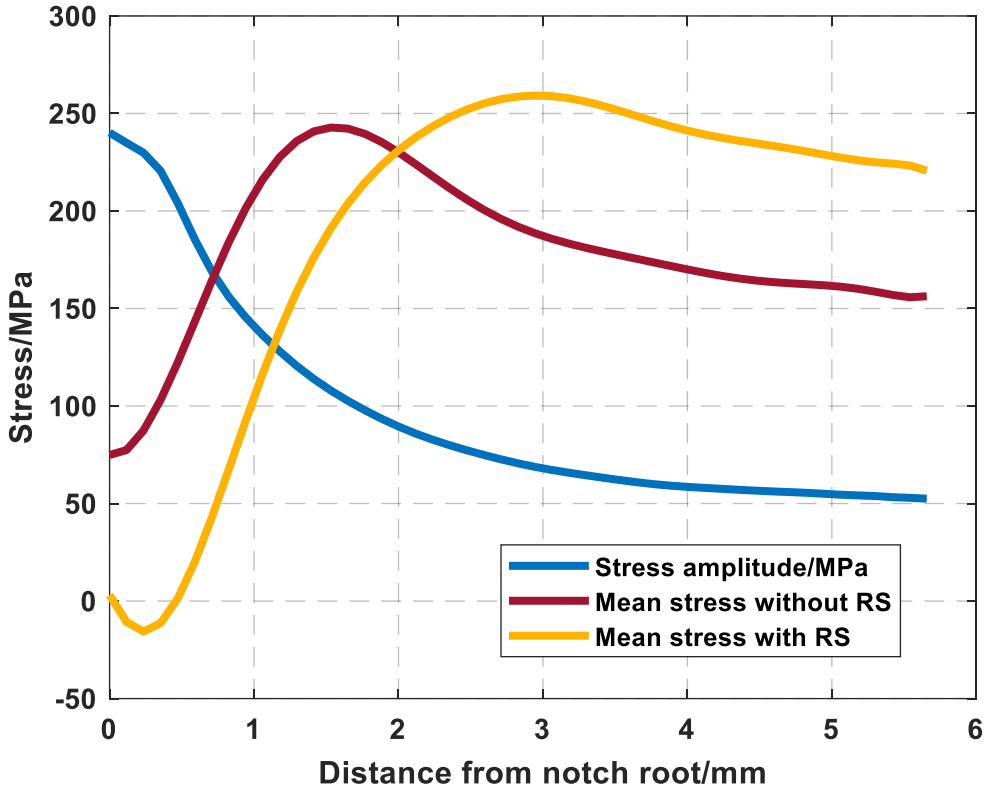

Figure 14. Stress amplitude and mean stress in notch region.

For no residual stress, the equivalent stress is calculated using the maximum stress amplitude shown as the red line in Figure 14. When residual is present, the mean stress shown as the yellow line in Figure 14 is used. The Walker Equation [32] is used to correlate the influence of mean stress:

$$\sigma_{ar} = \sigma_a(\frac{2}{1-R})^{1-\gamma} \tag{22}$$

where σ_{ar} is equivalent stress amplitude and γ is a material constant. The calculated σ_{ar} for force amplitude of 8kN, 8.5kN and 9kN are then substituted into S-N_i curve to obtain the crack initiation life with and without induced residual stress.

6 Experimental Investigation

Three 316LSS double-notch specimens with no induced residual stress and 5 specimens with a 21kN preload were tested under 8kN, 8.5kN and 9kN force amplitude (R=0) cyclic loads on a 100kN servo-hydraulic fatigue testing machine. All tests were under force control at 20 Hz. The test fatigue life results for the specimens with induced residual stress are shown in Figure 15, along with the fatigue life calculated using the proposed method.

In traditional stress-life fatigue analysis, prediction is based on a stress at a point. Averaged or nominal stress may be used at notch locations to account for stress gradient effects, but it is difficult to determine the appropriate characteristic length to obtain the average stress when residual stress is present, due to the variation in stress ratio. In such cases, the maximum stress is selected for substitution into the *S-N* curve, rather than an average stress. If the maximum stress amplitude is directly substituted into Huang's *S-N* curve, the predicted life is calculated as shown in Figure 15.

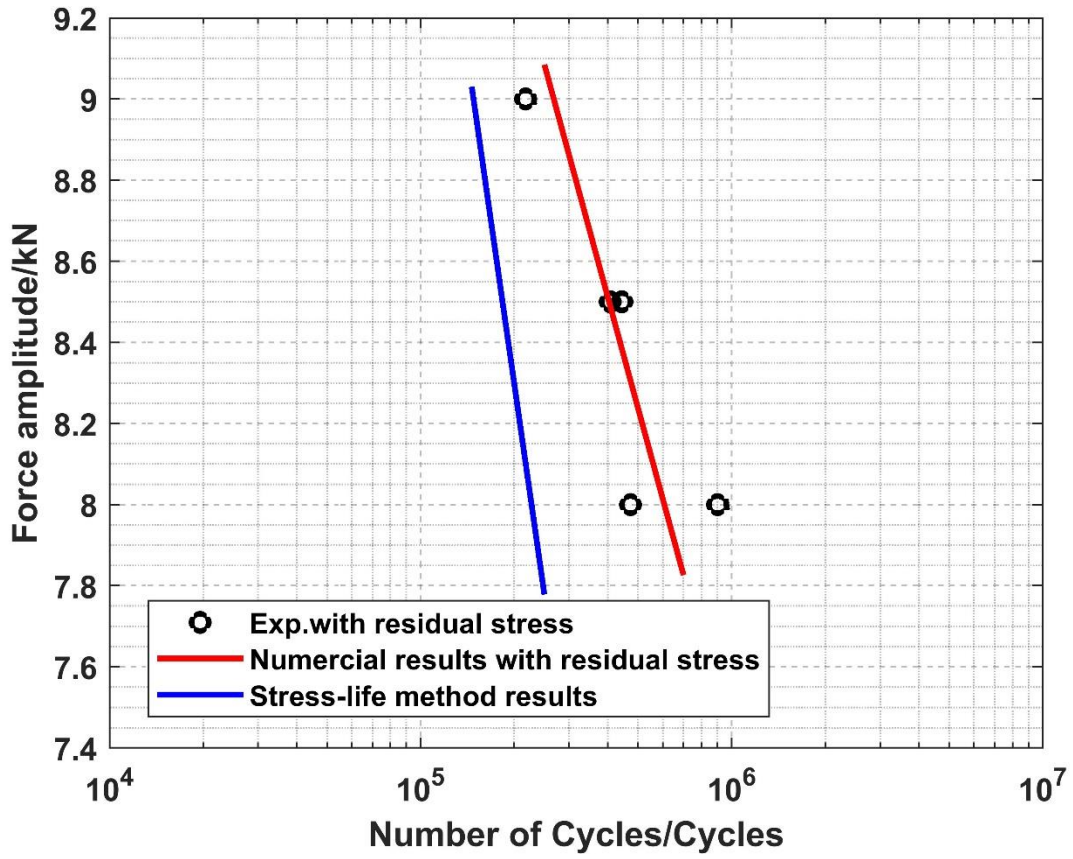

Figure 15. Calculated and experimental fatigue life for double-notch specimen with induced residual stress.

Both the proposed method and conventional stress-life method were also applied to fatigue life evaluation of specimens without residual stress. The numerical and experimental results are shown in Figure 16, which illustrates the beneficial effect of induced compressive residual stress on the fatigue life of the specimens. All numerical and experimental results are summarized in Figure 17, which shows that the traditional stress-life method results in underestimation of fatigue life and the proposed fracture mechanics method gives a closer approximation of the measured fatigue life.

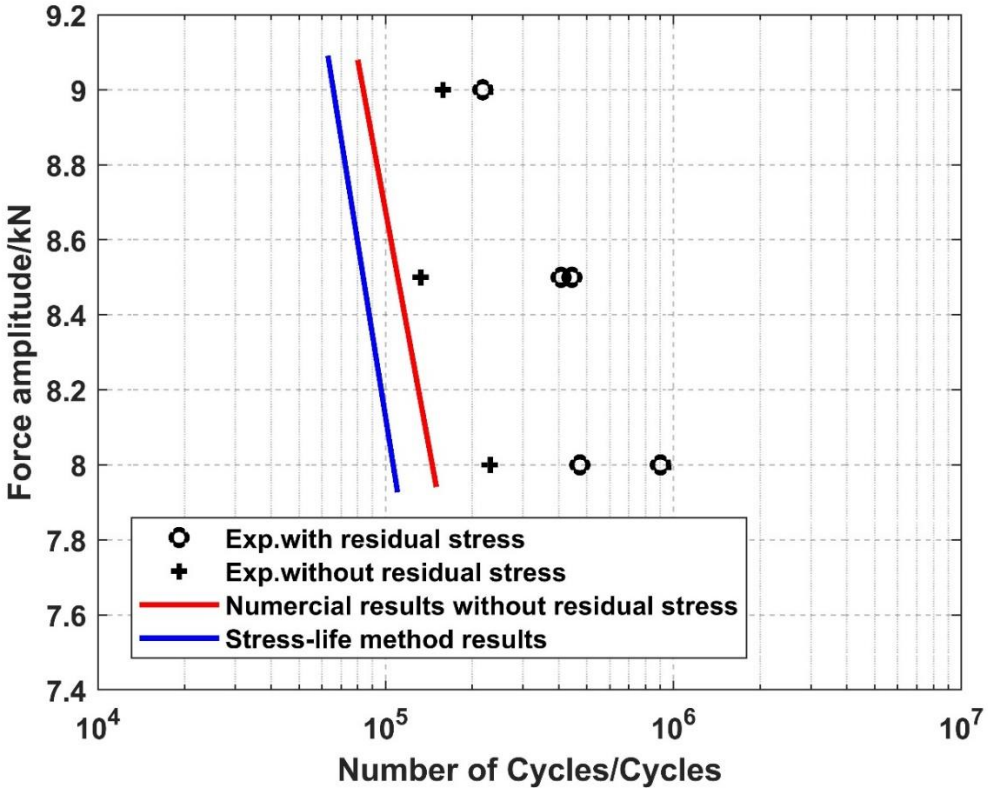

Figure 16. Calculated and experimental fatigue life for double-notch specimen with and without induced residual stress.

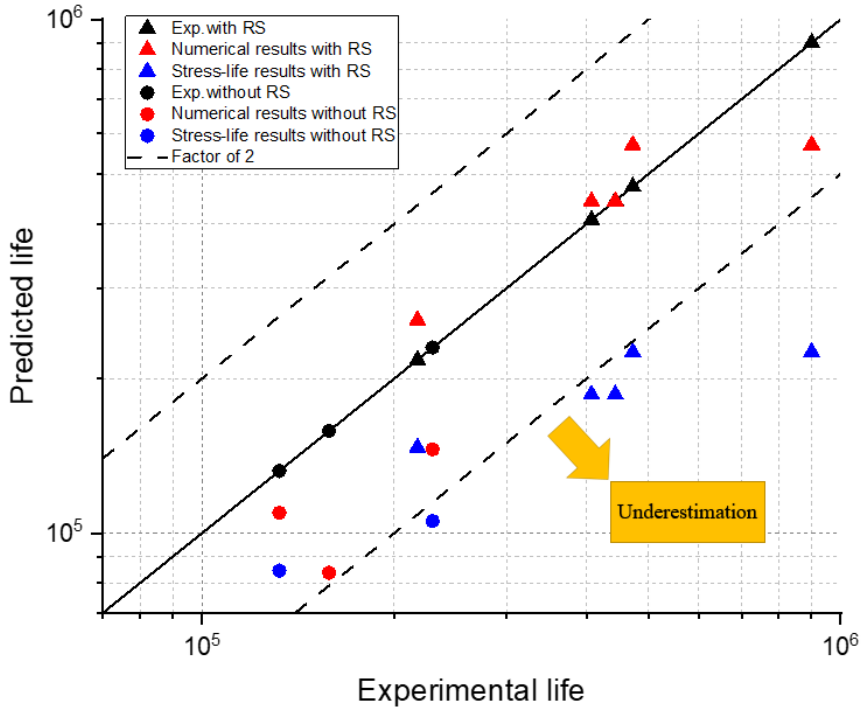

Figure 17. Comparison of calculated and experimental fatigue-life results.

7 Conclusion

The proposed method aims to enhance high cycle fatigue stress-life assessment of components with induced residual stress through application of a fracture mechanics crack growth model and a derived stress-crack initiation life curve. In the present numerical and experimental investigation, consideration is limited to 316L stainless steel. However, the method extends established fracture mechanics methods and is therefore expected to be appropriate for a high cycle fatigue analysis of other materials under a cyclic loading regime where LEFM is valid.

The analysis procedure requires definition of a material dependent initial crack length, proposed to be equivalent to the length of two material grains. For the 316L stainless steel, this length was assumed to be $200\mu m$. Based on the assumed crack initiation length, the number of cycles to crack initiation, N_i, is determined from a S-N_i curve obtained from standard S-N data and application of the ASNSYS SMART crack propagation tool. The assumed crack initiation length for other materials will vary depending on material grain size but may be defined in a similar manner.

The S-N_i curve can be used to determine crack initiation life of cyclically loaded components with both notch and residual stress effects. The crack propagation life of the component is evaluated by FEA, using the ANSYS Workbench SMART tool. In components with residual stress, the variation of stress intensity factor with increasing crack length is obtained in the form of polynomial equations and the crack propagation life obtained by superposition of the applied load stress distribution and residual stress distribution. The SMART crack growth tool is currently limited to linear elastic FEA, and the residual stress field resulting from preloading must be imported as an initial state of stress. The proposed method is not applicable to low cycle fatigue, in which plastic deformation may occur under the action of the cyclic external force after autofrettage.

Physical testing of double-notch 316L stainless steel specimens showed the expected enhanced fatigue life in specimens with induced residual stress. Application of the proposed method to analysis of specimens both with and without induced residual stress gave an improved estimation of fatigue life compared to the standard stress life approach. Further work is planned to investigate the validity of the method when applied to other materials and component configurations.

The method currently incorporates Physically Short Crack growth in the Long Crack growth model. More detailed consideration of the PSC would be expected to improve crack initiation

life prediction. A further area for investigation is the use of polynomial equations to define variation in stress intensity factors with crack length. This approach enables relatively simple application of the superposition method when calculating crack growth life for a varying stress ratio. However, minor differences in fracture parameters in the compressive residual stress region can significantly affect the calculated fatigue life, and further work is required to investigate the most appropriate fitting technique.

References

1. Shufen, R. and U.S. Dixit, *A review of theoretical and experimental research on various autofrettage processes.* Journal of Pressure Vessel Technology, 2018. **140**(5): p. 050802.
2. DOWLING, N.E., C.A. CALHOUN, and A. ARCARI, *Mean stress effects in stress-life fatigue and the Walker equation.* Fatigue & Fracture of Engineering Materials & Structures, 2009. **32**(3): p. 163-179.
3. Neuber, H., *Theory of notch stresses: principles for exact calculation of strength with reference to structural form and material*. Vol. 4547. 1961: USAEC Office of Technical Information.
4. Peterson, R. and R. Plunkett, *Stress concentration factors.* Journal of applied mechanics, 1975. **42**(1): p. 248.
5. Susmel, L. and D. Taylor, *A novel formulation of the theory of critical distances to estimate lifetime of notched components in the medium-cycle fatigue regime.* Fatigue & Fracture of Engineering Materials & Structures, 2007. **30**(7): p. 567-581.
6. Taylor, D., *The theory of critical distances.* Engineering Fracture Mechanics, 2008. **75**(7): p. 1696-1705.
7. Badr, E.A. and J. Ishak, *High-cycle fatigue behavior of type 4340 steel pressurized blocks including mean stress effect.* International Journal of Pressure Vessels and Piping, 2021. **194**: p. 104535.
8. Okorokov, V., et al., *High cycle fatigue analysis in the presence of autofrettage compressive residual stress.* Fatigue & Fracture of Engineering Materials & Structures, 2018. **41**(11): p. 2305-2320.
9. Hertel, O. and M. Vormwald, *Short-crack-growth-based fatigue assessment of notched components under multiaxial variable amplitude loading.* Engineering fracture mechanics, 2011. **78**(8): p. 1614-1627.
10. Hertel, O. and M. Vormwald, *Multiaxial fatigue assessment based on a short crack growth concept.* Theoretical and Applied Fracture Mechanics, 2014. **73**: p. 17-26.
11. Paris, P. and F. Erdogan, *A critical analysis of crack propagation laws.* 1963.
12. Needleman, A., *A continuum model for void nucleation by inclusion debonding.* 1987.
13. Belytschko, T. and T. Black, *Elastic crack growth in finite elements with minimal remeshing.* International journal for numerical methods in engineering, 1999. **45**(5): p. 601-620.
14. Moës, N., J. Dolbow, and T. Belytschko, *A finite element method for crack growth without remeshing.* International journal for numerical methods in engineering, 1999. **46**(1): p. 131-150.

15. Doğan, O., C. Yuce, and F. Karpat, *Effects of rim thickness and drive side pressure angle on gear tooth root stress and fatigue crack propagation life.* Engineering Failure Analysis, 2021. **122**: p. 105260.
16. Ignatijev, A., et al., *Fatigue crack initiation and propagation in a PM-gear tooth root.* Engineering Failure Analysis, 2022. **138**: p. 106355.
17. Lee, Y.F. and Y. Lu, *Advanced numerical simulations considering crack orientation for fatigue damage quantification using nonlinear guided waves.* Ultrasonics, 2022. **124**: p. 106738.
18. Bueckner, H., *Weight functions for the notched bar.* ZAMM‐Journal of Applied Mathematics and Mechanics/Zeitschrift für Angewandte Mathematik und Mechanik, 1971. **51**(2): p. 97-109.
19. Glinka, G. and G. Shen, *Universal features of weight functions for cracks in mode I.* Engineering Fracture Mechanics, 1991. **40**(6): p. 1135-1146.
20. Guo, K., R. Bell, and X. Wang, *The stress intensity factor solutions for edge cracks in a padded plate geometry under general loading conditions.* International journal of fatigue, 2007. **29**(3): p. 481-488.
21. Herz, E., O. Hertel, and M. Vormwald, *Numerical simulation of plasticity induced fatigue crack opening and closure for autofrettaged intersecting holes.* Engineering Fracture Mechanics, 2011. **78**(3): p. 559-572.
22. Santus, C. and D. Taylor, *Physically short crack propagation in metals during high cycle fatigue.* International Journal of Fatigue, 2009. **31**(8-9): p. 1356-1365.
23. Murthy, A.R., et al., *Prediction of fatigue crack initiation life in SA312 Type 304LN austenitic stainless steel straight pipes with notch.* Nuclear Engineering and Technology, 2022. **54**(5): p. 1588-1596.
24. Obrtlík, K., et al., *Short fatigue crack behaviour in 316L stainless steel.* International journal of fatigue, 1997. **19**(6): p. 471-475.
25. Brückner-Foit, A. and X. Huang, *Numerical simulation of micro-crack initiation of martensitic steel under fatigue loading.* International journal of fatigue, 2006. **28**(9): p. 963-971.
26. Pham, M. and S. Holdsworth, *Role of microstructural condition on fatigue damage development of AISI 316L at 20 and 300 C.* International journal of fatigue, 2013. **51**: p. 36-48.
27. Panda, B., et al., *Stress corrosion cracking in 316L stainless steel bellows of a pressure safety valve.* Engineering Failure Analysis, 2014. **36**: p. 379-389.
28. Dalla Palma, M., *Modelling of cyclic plasticity for austenitic stainless steels 304L, 316L, 316L (N)-IG.* Fusion Engineering and Design, 2016. **109**: p. 20-25.
29. Huang, J.-Y., et al., *High-cycle fatigue behavior of type 316L stainless steel.* Materials transactions, 2006. **47**(2): p. 409-417.
30. ASTM, E.-. *Standard practice for conducting force controlled constant amplitude axial fatigue tests of metallic materials.* West Conshohocken, 2021.
31. Toparli, M., A. Özel, and T. Aksoy, *Effect of the residual stresses on the fatigue crack growth behavior at fastener holes.* Materials Science and Engineering: A, 1997. **225**(1-2): p. 196-203.
32. Dowling, N.E., K.S. Prasad, and R. Narayanasamy, *Mechanical Behavior of Materials: Engineering Methods for Deformation, Fracture, and Fatigue*. 2013: Pearson.
33. Carpinteri, A., *Shape change of surface cracks in round bars under cyclic axial loading.* International Journal of Fatigue, 1993. **15**(1): p. 21-26.
34. Carpinteri, A., C. Ronchei, and S. Vantadori, *Stress intensity factors and fatigue growth of surface cracks in notched shells and round bars: two decades of research work.* Fatigue & Fracture of Engineering Materials & Structures, 2013. **36**(11): p. 1164-1177.

35. Elber, W., *The significance of fatigue crack closure.* 1971.
36. Newman Jr, J., *A crack opening stress equation for fatigue crack growth.* International Journal of fracture, 1984. **24**.
37. Ma, Y.E., et al., *Size effects on residual stress and fatigue crack growth in friction stir welded 2195-T8 aluminium–Part II: Modelling.* International Journal of Fatigue, 2011. **33**(11): p. 1426-1434.
38. Dinda, S. and D. Kujawski, *Correlation and prediction of fatigue crack growth for different R-ratios using Kmax and ΔK+ parameters.* Engineering Fracture Mechanics, 2004. **71**(12): p. 1779-1790.
39. ASTM, E., *Standard test methods for tension testing of metallic materials.* Annual book of ASTM standards. ASTM, 2021.
40. Gorash, Y. and D. MacKenzie, *On cyclic yield strength in definition of limits for characterisation of fatigue and creep behaviour.* Open Engineering, 2017. **7**(1): p. 126-140.
41. Khan, A.S., A. Pandey, and T. Stoughton, *Evolution of subsequent yield surfaces and elastic constants with finite plastic deformation. Part III: Yield surface in tension–tension stress space (Al 6061–T 6511 and annealed 1100 Al).* International Journal of Plasticity, 2010. **26**(10): p. 1432-1441.
42. Michno Jr, M.J. and W.N. Findley, *An historical perspective of yield surface investigations for metals.* International Journal of Non-Linear Mechanics, 1976. **11**(1): p. 59-82.
43. Ishikawa, H., *Subsequent yield surface probed from its current center.* International Journal of Plasticity, 1997. **13**(6-7): p. 533-549.
44. Abdel-Karim, M., *Effect of elastic modulus variation during plastic deformation on uniaxial and multiaxial ratchetting simulations.* European Journal of Mechanics-A/Solids, 2011. **30**(1): p. 11-21.
45. Prager, W., *A new method of analyzing stresses and strains in work-hardening plastic solids.* 1956.
46. Armstrong, P.J. and C. Frederick, *A mathematical representation of the multiaxial Bauschinger effect*. Vol. 731. 1966: Berkeley Nuclear Laboratories Berkeley, CA.
47. Chaboche, J., K.D. Van, and G. Cordier, *Modelization of the strain memory effect on the cyclic hardening of 316 stainless steel.* 1979.
48. Dutta, A., S. Dhar, and S. Acharyya, *Material characterization of SS 316 in low-cycle fatigue loading.* Journal of Materials Science, 2010. **45**(7): p. 1782-1789.
49. Xie, X.-f., et al., *Cyclic hardening/softening behavior of 316L stainless steel at elevated temperature including strain-rate and strain-range dependence: Experimental and damage-coupled constitutive modeling.* International Journal of Plasticity, 2019. **114**: p. 196-214.
50. Schijve, J., *The stress intensity factor of small cracks at notches.* Fatigue & Fracture of Engineering Materials & Structures, 1982. **5**(1): p. 77-90.